

# High-Throughput Screening on Halide Perovskite Derivatives and Rational Design of $\text{Cs}_3\text{LuCl}_6$

Hyeon Woo Kim,<sup>†</sup> Joo Hyeong Han,<sup>†</sup> Hyunseok Ko,<sup>†</sup> Tuhin Samanta, Dong Geon Lee, Dong Won Jeon, Woongchan Kim, Yong-Chae Chung, Won Bin Im,\* and Sung Beom Cho\*



Cite This: *ACS Energy Lett.* 2023, 8, 3621–3630



Read Online

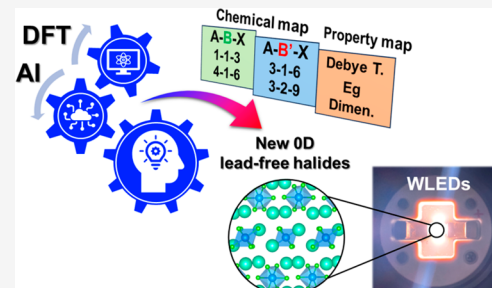
ACCESS |

Metrics & More

Article Recommendations

Supporting Information

**ABSTRACT:** Exploring the vast and veiled chemical spaces via synthesis is essential in solid-state materials. However, navigating uncharted chemical spaces can be a daunting task, particularly when a material has complex structural features. Metal halides represent one such space, where the coexistence of perovskites and their derivatives has restricted the exploration of this fascinating family. Here, we meticulously collect inorganic halide perovskite derivatives and systematically explore them via a combination of high-throughput density functional theory calculations and machine learning. We chart the chemical spaces by listing stable compositions on the periodic table and yield informatics on electrical properties and thermal stability. Guided by these predictions, we showcase the successful synthesis of new  $\text{Cs}_3\text{LuCl}_6$ , as well as its implementation into white-light-emitting diodes. Our exploration can inspire the design of inorganic metal halides, thereby paving the way for envisioning their practical applications across various fields.



Halide perovskites have emerged as promising materials due to their excellent optoelectronic properties, ease of fabrication, and low-cost production. They are showing state-of-the-art performances in various applications such as photovoltaics,<sup>1,2</sup> photodetectors,<sup>3,4</sup> light-emitting diodes (LEDs),<sup>5,6</sup> lasers,<sup>7</sup> thin-film transistors,<sup>8</sup> and so on. These optoelectronic applications are attributed to their unique optical and electronic properties such as superior light harvesting capability, high photoluminescence quantum yields (PLQYs), narrow emission width, and high charge carrier mobility.<sup>9</sup> However, despite their remarkable progress, this material class still faces several limitations. The current state of halide perovskites is marked by instability, as they are susceptible to environmental factors such as moisture, oxygen, and heat, leading to rapid degradation and compromising their long-term performance. Additionally, the presence of toxic elements like lead in their composition raises concerns about environmental and human health risks. Numerous efforts are being made to address these issues, and recent research has focused on developing alternative materials and improving stability through compositional engineering, encapsulation techniques, and optimization of fabrication processes.

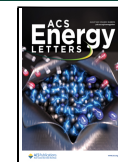
Recently, all-inorganic halide perovskites are being considered as an alternative to the conventional halide perovskites. The conventional  $\text{ABX}_3$  perovskite structure has 3D connectivity of  $\text{BX}_6$  octahedra; however, such a polyhedral

connectivity in perovskite derivatives can be reduced to 2D, 1D, or even 0D by choosing a heterovalent B ion (replacing  $\text{Pb}^{2+}$ ) or changing the stoichiometry. This reduction of connectivity can enhance their environmental stability, improve moisture resistance, and allow for tunable bandgaps, which make them promising candidates for various optoelectronic applications.<sup>10,11</sup> The example cases are  $\text{Cs}-\text{Mn}-\text{Cl}$ <sup>12</sup> in  $\text{A}_2\text{B}_1\text{X}_4$ ,  $\text{Cs}-\text{Tb}-\text{Cl}$ <sup>13</sup> and  $\text{Cs}-\text{Sc}-\text{Cl}$ <sup>14</sup> in  $\text{B}_3\text{B}_1\text{B}_6$ , and so on. Their compositional diversity and structural dimensionality,<sup>15,16</sup> however, require numerous efforts to explore novel materials in almost infinite chemical spaces despite their promising potentials.<sup>17–19</sup> Thereby the development in the field of perovskite derivatives is still in its infancy, necessitating further systematic investigations, including the integration of machine learning (ML) and density functional theory (DFT) computations.<sup>20,21</sup> In addition, understanding low-dimensional inorganic metal halides' physical and chemical nature still remains a mystery.<sup>22</sup> The challenges of gaining insights into

Received: June 18, 2023

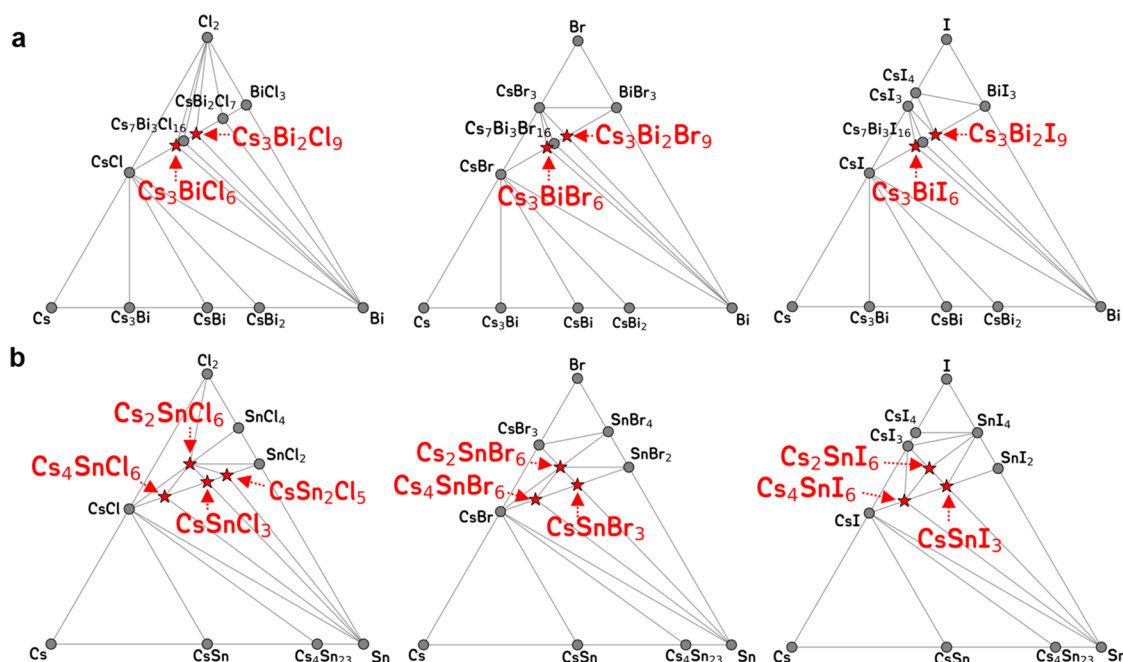
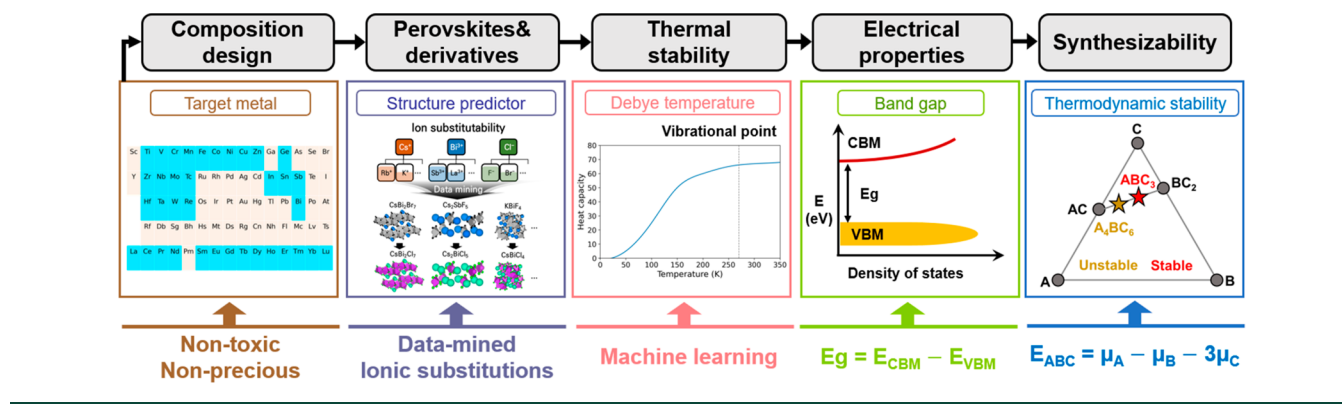
Accepted: July 28, 2023

Published: August 2, 2023



ACS Publications

© 2023 American Chemical Society

**Scheme 1.** Workflow of Computational Exploration for Inorganic Halide Perovskite Derivatives

**Figure 1.** DFT-calculated 0 K phase diagram of (a) Cs-Bi-X and (b) Cs-Sn-X systems (where X = Cl, Br, and I). The red dots correspond to stable ternary compounds that match the stoichiometries in the synthesis reports.

the design and synthesis of inorganic metal halides have largely contributed to the lack of known materials in this class. These knowledge constraints also present significant risks to the exploratory synthesis of overall inorganic metal halide materials.

In this work, we undertake a computational material exploration for inorganic ternary halide perovskites and their derivatives, incorporating experimental synthesis. Through case studies of Cs-Bi-X and Cs-Sn-X systems, we assess the feasibility of collecting perovskites and their derivatives. Subsequently, we apply this approach to investigate 108 metal halide systems (transition metals, post-transition metals, and lanthanides for metals, and chlorine, bromine, and iodine for halides), resulting in 1703 multi-dimensional structures ranging from 3D to 0D. Employing high-throughput DFT calculations and ML, we unveil significant trends in thermal stability and electrical properties, sorted by metal and halide groups. These trends offer concise and accessible insights. Furthermore, we map the chemical space by listing thermodynamically stable compositions on a periodic table, enabling a comprehensive understanding of the uncharted material landscape. Notably, our exploration led to the

identification of 153 previously unknown materials. Among them, we pinpoint a new metal halide, Cs<sub>3</sub>LuCl<sub>6</sub>, which we successfully synthesized and verified. Moreover, we demonstrate its practical application in a white-light-emitting diode. Beyond conventional halide perovskites, our study sheds light on previously unexplored derivatives, characterized by their structural diversity and chemical complexity, thereby inspiring further investigation into the advance of metal halides for optoelectronics and other practical applications.

The overall process for computational exploration was organized into five steps, as shown in Scheme 1. As a first step, the chemical space of A-B-X element combinations was selected as follows. For the A-site cation, we adopted only Cs because it is a comprehensive element that can serve as a reference for other alkali ions like Rb, K, and Na, as well as organic cations and pseudohalides. Next, for the B-site cation, we considered a lead-free series to find alternatives for toxic lead. Generally, Sn, Sb, Ge, and Bi are known as conventional lead-free elements.<sup>18,19</sup> In addition to these, new lead-free series have recently been discovered in transition metals,<sup>14,23–26</sup> post-transition metals,<sup>8,27–30</sup> and even lanthanides.<sup>13,31,32</sup> These series exhibit moderate environmental

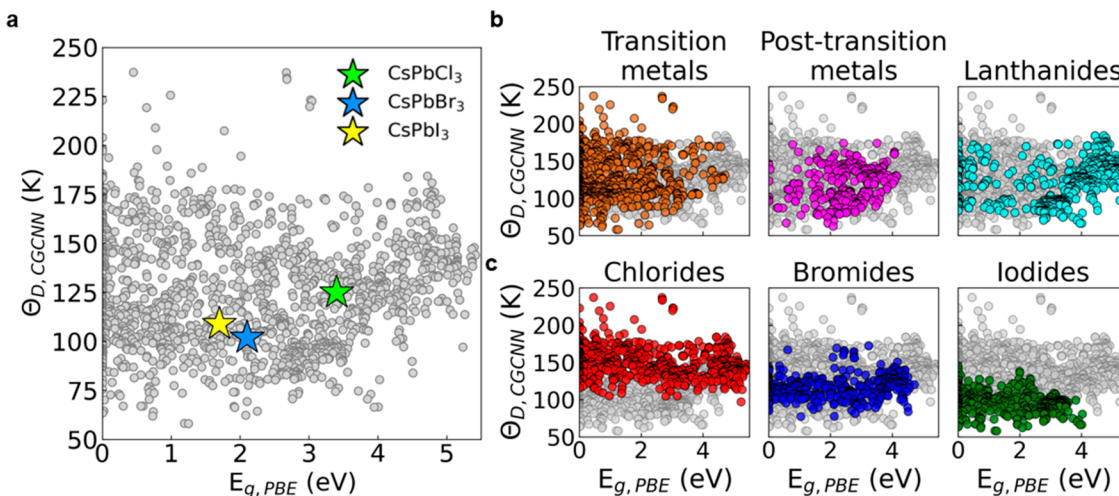


**Figure 2.** CGCNN-predicted Debye temperature ( $\Theta_{D,CNN}$ ) with PBE-calculated band gap ( $E_{g,PBE}$ ) for (a) halides, (b) transition metals, post-transition metals, and lanthanides, and (c) chlorides, bromides, and iodides. The light green, cobalt, and yellow stars indicate data for  $CsPbCl_3$ ,  $CsPbBr_3$ , and  $CsPbI_3$ , respectively, extracted from the literature.<sup>66,67</sup>

stability with usable optoelectronic performance but are still extremely uncommon. Hence, 36 lead-free metals encompassing transition metals, post-transition metals, and lanthanides were selected as the B-site cations, excluding certain precious and toxic elements. This selection resulted in the achievement of a composition space of 108 Cs-B-X combinations.

As the next step, we built a material repository to explore inorganic halide perovskites and their multiplex derivatives. Our strategy for building a repository is to merge the previously reported and hypothetically generated crystal structures. The former involves mining already existing ternary metal halides, and the latter concentrates on exploring undiscovered ternary metal halides. In other words, perovskite and conventional derivatives are gathered via data mining, whereas uncommon derivatives are captured virtually. We first collect common crystal structures of ternary metal halides by data-mining the already-known experimental and computational domains from the Inorganic Crystal Structure Database (ICSD) and DFT-based databases.<sup>33,34</sup> Subsequently, we use a structure prediction method based on ionic substitutability to construct a hypothetical crystal structure.<sup>35</sup> This approach statistically probes commensurate chemical substitutions on our target element combinations and takes their known crystal structures as prototypes. Then, they are substituted with the target elements, and finally, novel but plausible candidate material phases are generated.<sup>36–39</sup> It also enables the creation of multiphases derived by multiple oxidation states, e.g., Sn with +2 and +4. Hence all possible oxidation states of 36 lead-free metals are considered to meticulously generate the hypothetical structure, as shown in Table S1. We also eliminate duplicate structures in a material repository by filtering structurally similar compounds with the PyMatGen structure matcher.<sup>40</sup>

Prior to building a material repository and conducting large-scale DFT calculations, we performed a validation of the collection process for inorganic halide perovskites and their derivatives. This involved utilizing the aforementioned methods alongside DFT calculations to assess the thermodynamic stability<sup>41</sup> of computationally predicted ternary metal halides. Our focus was on comparing these predicted compounds with previously synthesized materials, taking into account stoichiometric matches resulting from the synthetic

procedures. Note that in instances where a crystal structure was clearly reported in experimental studies, we conducted a direct comparison with our calculated structures. To conduct this assessment, we specifically carried out case studies for Cs-Bi-X and Cs-Sn-X, as there are comparatively abundant synthesis reports among inorganic lead-free halides.

Figure 1 shows the DFT-calculated 0 K phase diagram for Cs-Bi-X and Cs-Sn-X cases, highlighting the stable ternary metal halides that align with consistent experimental reports. As shown in Figure 1a, we found that several stable ternary metal halides in Cs-Bi-X case were consistent with previous synthesis reports for  $Cs_3BiCl_6$ ,  $Cs_3Bi_2Cl_9$ ,  $Cs_3BiBr_6$ ,  $Cs_3Bi_2Br_9$ ,  $Cs_3BiI_6$ , and  $Cs_3Bi_2I_9$ .<sup>16,42–46</sup> Although no synthesis reports currently exist for a few other stable compounds ( $Cs_7Bi_3Cl_{16}$ ,  $Cs_2Bi_2Cl_7$ ,  $Cs_7Bi_3Br_{16}$ , and  $Cs_7Bi_3I_{16}$ ), their absence in the literature could be attributed to a variety of factors. It is possible that alternative compositions with more favorable stability are preferentially formed, or that kinetic processes during synthesis hinder their formation.<sup>47</sup> For the Cs-Sn-X case, as shown in Figure 1b, we confirmed that it agreed well with synthesis reports, including those for  $CsSnCl_3$ ,  $CsSn_2Cl_5$ ,  $Cs_2SnCl_6$ ,  $Cs_4SnCl_6$ ,  $CsSnBr_3$ ,  $Cs_2SnBr_6$ ,  $Cs_4SnBr_6$ ,  $CsSnI_3$ ,  $Cs_2SnI_6$ , and  $Cs_4SnI_6$ .<sup>29,30,48–55</sup> Despite the complexity of multiphase presence due to multivalent Sn atoms with +2 and +4, the 10 perovskites and derivatives collected above were validated. This demonstrates that our approach is not only thorough in collecting even the elusive perovskite derivatives but also plausible in predicting the synthesizability of halides. Hence, we generated 1703 distinct metal halides from 108 Cs-B-X elements combinations (as summarized in Figure S1) and then computed them via high-throughput DFT calculations.

Debye temperature ( $\Theta_D$ ) is a key parameter that characterizes the vibrational properties of materials. It plays a significant role as an indicator in thermally robust applications, particularly in fields such as LEDs.<sup>36,56</sup>  $\Theta_D$  also gives indirect information on light-emitting performances associated with heat degradation in inorganic halide-based optoelectronics applications.<sup>57–59</sup> DFT calculations possess the capability to predict  $\Theta_D$ , but applying them to large-scale materials presents challenges due to the enormous computational resources needed. To overcome this, we used Crystal Graph Convolutional Neural Networks (CGCNN),<sup>60</sup> a ML approach capable

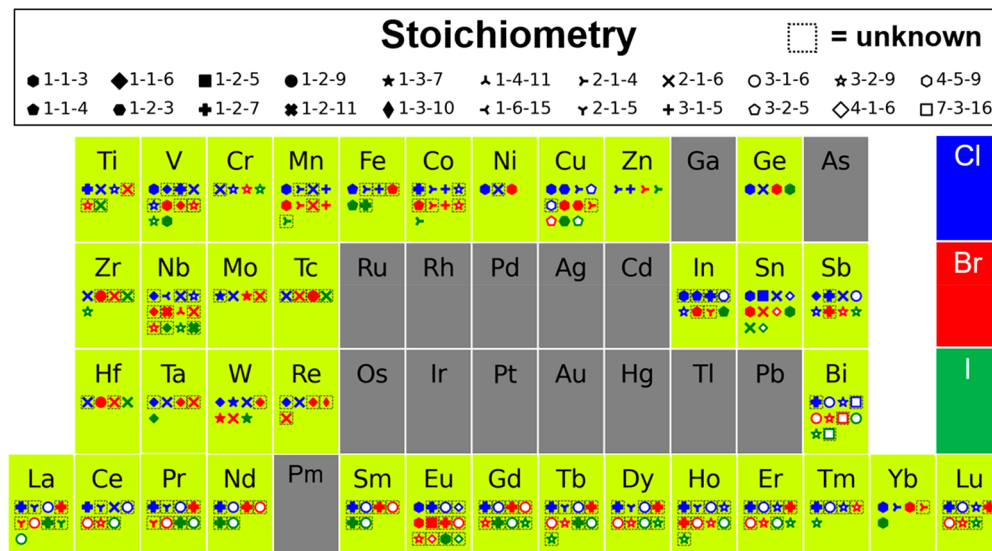


**Figure 3.** A periodic table of the stable Cs-B-X system. Blue, red, and green markers are chloride, bromide, and iodide, respectively. The dotted squares indicate unknown stoichiometry in the ICSD.

of predicting material properties using only the crystal structure and chemical composition. CGCNN uses the associated atomic structure and stoichiometry, as well as known property data, to train a prediction model. Subsequently, this trained model can swiftly predict the properties based solely on atomic structure and stoichiometry, thereby facilitating an accelerated exploration of new materials.<sup>61</sup> Hence, we extracted pre-calculated  $\Theta_D$  data at the DFT level<sup>62</sup> and pre-processed them (*Supporting Information 2*) to enhance prediction performance (*Figure S2*). Comparative analysis of experiments, DFT, and CGCNN predictions revealed comparable prediction accuracy (*Figure S3*). Leveraging the DFT-optimized crystal structure, we successfully obtained  $\Theta_D$  values for 1703 cesium-based ternary metal halides without enormous computational resources.

Another important property is the band gap, which directly decides how the materials interact with light. The band gap is also relevant to the performance and reliability of optoelectronic devices, especially for indirect types, as phonon-generated heat during energy transition can lead to efficiency losses and thermal degradation. It has hence been controlled through strategies like alloying or doping in optoelectronics applications.<sup>63–65</sup> In the case of metal halides, the band gap is mainly determined by the B–X bond and the polyhedral features. Moreover, these crystallographic properties are versatile, depending on the types of metals and anions. Thus, we extracted the band gap of 1703 cesium-based ternary metal halides to map their overall distributions by group. The extraction was performed with a PBE functional, which tends to underestimate the band gap; still, it is suitable for capturing trends in large-scale materials.<sup>36,56</sup> Subsequently, for certain candidates, the HSE functional is used to achieve accurate band gap determination.

**Figure 2a** displays the results for 1703 cesium-based ternary metal halides with PBE band gaps ranging from 0 to 5.5 eV and  $\Theta_D$  from 50 to 250 K. These ranges included all values.  $\Theta_D$  is the temperature at which the crystal lattice begins to vibrate with increasing amplitude and is, hence, correlated with the thermal robustness of the material. The  $\text{CsPbX}_3$  series was marked to guide our predictions, and we found that it exhibits

poor thermal stability among inorganic metal halide perovskites, consistent with thermal instability issues.<sup>5</sup> Thus, it was confirmed that several thermally robust inorganic lead-free halides exist beyond this series. We also plotted sorting diagrams for each group of elements to study their composition-dependent impacts on properties. **Figure 2b** shows the distribution of the Debye temperature and the band gap. For the B-site cation groups, the Debye temperature was comparable across metal groups, whereas the band gap exhibited varying tendencies based on the transition metal, post-transition metal, and lanthanides. Although a comparison of the thermal stability between the B-site cation groups requires more in-depth analysis in the future, we emphasize that this intuitive visualization is informative, especially for relatively unexplored lanthanides. In contrast to sorting for the B-site cation groups, the X-site anion groups showed a clear trend of decreasing the band gap and the Debye temperature in the order of chlorides, bromides, and iodides, as demonstrated in **Figure 2c**. We speculate that this tendency is partially correlated by the difference in atomic radius between halide anions, since smaller atomic radii allow a wide band gap and dense polyhedral packing.<sup>56,68</sup> These predictions can guide engineering strategies, such as alloying and doping, that enable tuning of both thermal robustness and electrical properties.<sup>69,70</sup>

Exploring uncharted compositional spaces can assist to guide experimental synthesis efforts and thereby be applied to capture the inspiration toward discovery of novel materials that have yet to be found.<sup>37</sup> Moreover, the persistent scarcity of known compounds remains a significant bottleneck and limitation in material design. Metal halides are one of the still-hidden chemical spaces due to their multi-dimensional structural nature.<sup>17,71</sup> The energy above hull, one of the factors in assessing synthesizability, is useful for exploring chemical space via screening vast materials.<sup>36</sup> This factor indicates the thermodynamic driving force for a compound to decompose.<sup>72,73</sup> To evaluate this factor, we used the DFT-calculated energy of 1703 cesium-based ternary metal halides. We identified 255 compounds with an energy of 0 meV/atom,

**Table 1.** 16 New Types of Low-Dimensional Cesium-Based Ternary Metal Halides Discovered from Computational Exploration

Composition	ICSD	$E_{\text{hull}}$ (meV/atom)	$\Theta_{D,\text{CGCNN}}$ (K)	$E_g$ , PBE (eV)	$E_g$ , HSE (eV)	$E_g$ type	Dimension
Cs <sub>3</sub> Co <sub>2</sub> Cl <sub>9</sub>	×	0	168	1.15	3.35	Direct	0
CsLu <sub>2</sub> Cl <sub>7</sub>	×	0	165	4.84	6.49	Direct	2
CsW <sub>3</sub> Br <sub>7</sub>	×	0	165	2.75	3.92	Direct	0
CsDy <sub>2</sub> Cl <sub>7</sub>	×	0	159	4.70	6.22	Direct	2
CsLa <sub>2</sub> Cl <sub>7</sub>	×	0	156	4.28	6.24	Direct	2
CsEr <sub>2</sub> Cl <sub>7</sub>	×	0	154	4.75	6.33	Direct	2
CsNd <sub>2</sub> Cl <sub>7</sub>	×	0	154	4.57	5.96	Direct	2
CsHo <sub>2</sub> Cl <sub>7</sub>	×	0	153	4.73	6.28	Direct	2
CsGd <sub>2</sub> Cl <sub>7</sub>	×	0	153	2.67	5.99	Direct	2
CsSm <sub>2</sub> Cl <sub>7</sub>	×	0	152	4.61	6.04	Direct	2
Cs <sub>3</sub> LuCl <sub>6</sub>	×	0	149	5.14	6.45	Direct	0
CsPr <sub>2</sub> Br <sub>7</sub>	×	0	148	3.62	4.97	Direct	2
Cs <sub>4</sub> Cu <sub>5</sub> Cl <sub>9</sub>	×	0	147	1.90	3.46	Direct	1
Cs <sub>4</sub> EuCl <sub>6</sub>	×	0	146	1.19	3.53	Direct	0
CsVCl <sub>6</sub>	×	0	146	1.01	2.10	Direct	0
CsTm <sub>2</sub> Cl <sub>7</sub>	×	0	145	4.78	6.38	Direct	2

indicating they are thermodynamic ground states and highly probable for experimental synthesis.

By directly observing the crystal structure of stable compounds, we evaluated their dimensionality to identify structural features (Figure S4). Perovskite accounted for less than 10% of the total structures, while derivatives were overwhelmingly abundant. Notably, the 0D structure dominates the sample of derivatives, and 1D and 2D structures are more abundant than 3D structures. This finding indicates that the uncharted compositional space of metal halides is due to the structural diversity driven by the multi-dimensional nature, supporting the significance of exploring perovskite derivatives.

To visualize the list of synthesizable chemical compositions, Figure 3 shows a periodic table charting the stable compounds, colored for classification by halides and highlighted if they do not exist in the ICSD. Among the 255 stable compounds, there were 109 stable chlorides and 90 bromides, which suggests a potential for diverse compositional designs compared to the 56 stable iodides. It was also identified that the not-yet-synthesized stoichiometries included 53 out of 109 for transition metals, 12 out of 40 post-transition metals, and 88 out of 106 lanthanides. These findings suggest an incomplete exploration of inorganic lead-free halides, highlighting the need for extensive further experimental synthesis efforts, particularly focusing on rare earth elements, to advance our understanding in this area. This table also showcases 22 distinct stoichiometries that can be combined within the Cs-B-X compositional space. The main stoichiometric ratios according to the oxidation states of the B-site cation metals were found in the following order: +1 in 1-2-3 and 3-2-5, +2 in 1-1-3 and 2-1-4, +3 in 3-1-6 and 3-2-9, +4 in 2-1-6, and +5 in 1-1-6 (Figure S5). Excluding these, minor stoichiometries are offered in more detail (Figure S6). Overall, our findings provide insights into the material design for inorganic lead-free halides, guiding exploratory synthesis in new chemical spaces.

In our pursuit of discovering new materials through computational exploration, experimental validation, and envisioning their practical applications, we embarked on an extensive investigation of 1703 cesium-based ternary metal halides. This exploration involved screening DFT-calculated and CGCNN-predicted properties, with the objective of identifying materials that exhibit characteristics comparable

to those of the CsPbX<sub>3</sub> series. The details of the screening process are explained in the SI (supplementary notes 1 and Figure S7). From this screening, we identified 16 candidates with properties which are listed in Table 1. Among them, we focused on the 0D metal halides because they recently exhibited fascinating optical characteristics with the excitonic emission feature, as well as robust thermal stability.<sup>10</sup> We pinpointed Cs<sub>3</sub>LuCl<sub>6</sub> as a candidate for a successful experimental validation. While CsW<sub>3</sub>Br<sub>7</sub> and Cs<sub>3</sub>Co<sub>2</sub>Cl<sub>9</sub> exhibited higher  $\Theta_D$ , their synthetic routes are narrow due to the multivalent nature of W and Co, complicated by the established knowledge that they are not commonly employed as luminescent materials, resulting in their exclusion from further consideration. In contrast, Cs<sub>3</sub>LuCl<sub>6</sub>, a trivalent pure phase, was thermally stable and showed a direct band gap. Notably, lutetium is an under-explored element. We also anticipate that its functionalization can be achieved via the implementation of a doping strategy, which can effectively augment the properties of metal halides.<sup>74</sup> Consequently, further synthesis and characterization to validate our work will target new the Cs<sub>3</sub>LuCl<sub>6</sub>.

Cesium lutetium chloride, Cs<sub>3</sub>LuCl<sub>6</sub>, was synthesized through a solid-state reaction and hot injection methods. Cs<sub>3</sub>LuCl<sub>6</sub> metal halide has a 0D crystal structure consistent with the calculated results, belonging to the monoclinic C2/c space group and including LuCl<sub>6</sub> octahedra (Figure 4a). The centers of Lu1 and Lu2 octahedra and their Lu–Cl bond lengths are shown in Figure 4b,c. The material was synthesized as polycrystalline phases through a solid-state reaction, and a detailed description of the synthesis is included in the Supporting Information. The structure of Cs<sub>3</sub>LuCl<sub>6</sub> was analyzed using powder X-ray diffraction (XRD), and the XRD data were refined using the GSAS software suite for a comprehensive verification of the structure. The refined lattice parameters and atomic positions of Cs, Cl, and Lu are listed in Tables S2 and S3. The refined parameters indicated that the XRD pattern of the Cs<sub>3</sub>LuCl<sub>6</sub> (Figure 4d) metal halide matched well with the simulated result. The chemical properties of Cs<sub>3</sub>LuCl<sub>6</sub> were further confirmed by using X-ray photoelectron spectroscopy (XPS). The full-range XPS spectrum is shown in Figure 4e, with the characteristic peaks of Cs 3d, Lu 4p, and Cl 2s indicating that Lu is in the +3-

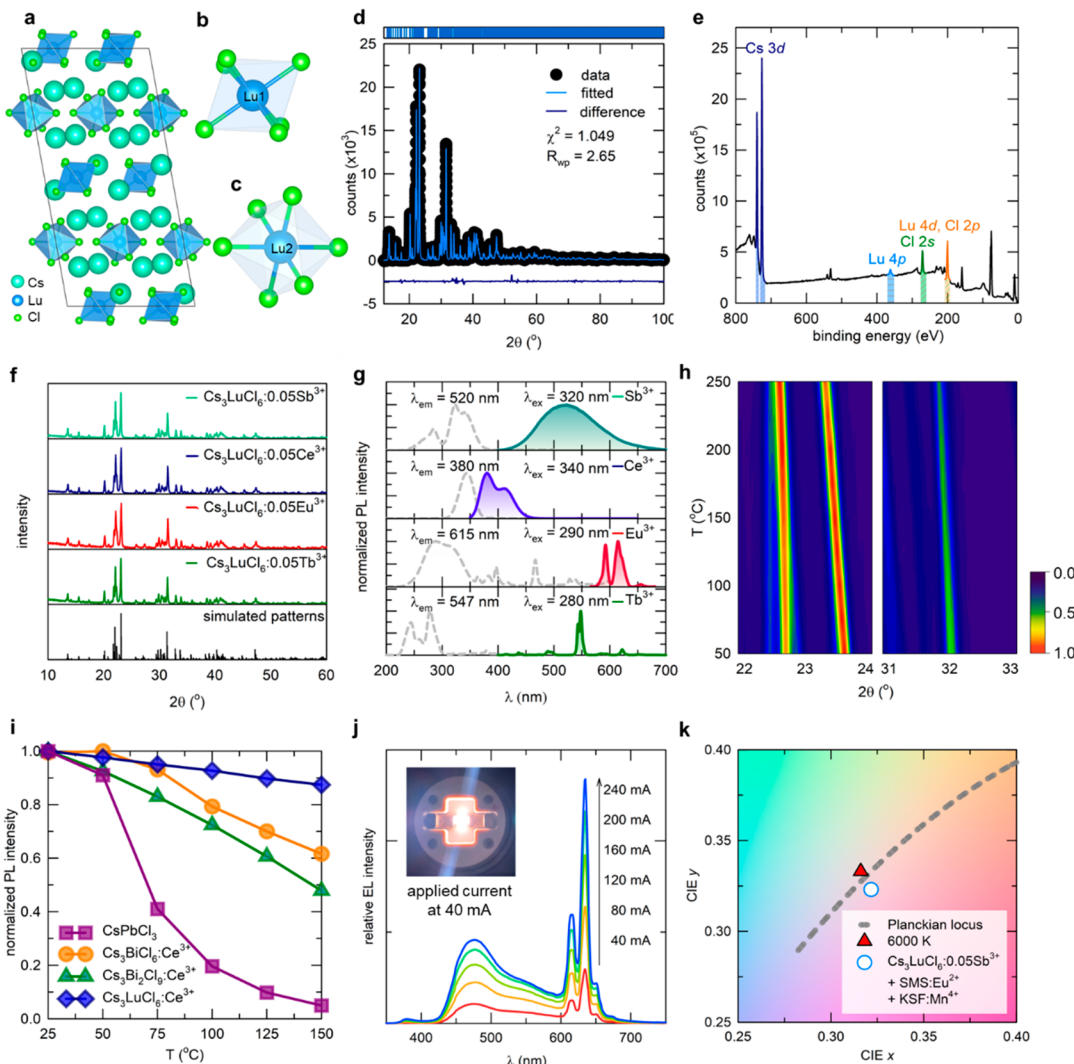


**Figure 4.** (a) Crystal structure of  $\text{Cs}_3\text{LuCl}_6$  in the [001] direction. (b,c) Octahedral sites of  $\text{LuCl}_6$ . (d) Observed (dots), calculated (blue), and difference (deep blue) profiles obtained after full-pattern Rietveld refinement of  $\text{Cs}_3\text{LuCl}_6$  polycrystals. (e) Full-range XPS survey spectra of the different elements of  $\text{Cs}_3\text{LuCl}_6$ . (f) XRD patterns of different activators in  $\text{Cs}_3\text{LuCl}_6$  polycrystals. (g) PL, PLE spectra, and luminescence images of  $\text{Cs}_3\text{LuCl}_6$  polycrystals with different activators. (h) Temperature-dependent XRD patterns of  $\text{Cs}_3\text{LuCl}_6$  polycrystals. (i) Temperature-dependent PL intensity comparison of  $\text{Cs}_3\text{LuCl}_6:0.05 \text{Ce}^{3+}$  with  $\text{CsPbCl}_3$ ,  $\text{Cs}_3\text{BiCl}_6:0.05 \text{Ce}^{3+}$ , and  $\text{Cs}_3\text{Bi}_2\text{Cl}_9:0.05 \text{Ce}^{3+}$ . (j) EL spectra and the image of fabricated WLED using  $\text{Cs}_3\text{LuCl}_6:0.05 \text{Sb}^{3+}$  as the green component. (k) CIE chromaticity coordinates of the fabricated  $\text{Cs}_3\text{LuCl}_6:0.05 \text{Sb}^{3+}$  prototype WLED.

oxidation state in the metal halide. The  $\text{Cl } 2p$  and  $\text{Lu } 4d$  peaks overlap, and the high-resolution XPS spectra for this are detailed in Figure S8. In addition, scanning electron microscopy (SEM) photographs of highly crystalline  $\text{Cs}_3\text{LuCl}_6$  are shown in Figure S9a, indicating the formation of irregular polycrystals with particle sizes in the range of approximately 10  $\mu\text{m}$ . The elemental energy-dispersive X-ray spectroscopy (EDAX) mapping in Figure S9b,d shows a uniform distribution of Cl, Cs, and Lu throughout the material.

We also synthesized  $\text{Cs}_3\text{LuCl}_6$  in nanocrystal form and conducted XRD analysis to confirm the successful synthesis using the hot injection method. In Figure S10a, XRD patterns show that the synthesized crystal structure matches the simulated one. As seen in Figure S10b, the synthesized nanocrystals have a distorted ellipse shape. The distance between planes identified by the high-resolution transmission electron microscope (HR-TEM) image is shown in Figure S10c. The distance between (404) planes was 0.27 nm and

matched with XRD results. Size distribution analysis, shown in Figure S10d, confirmed that the nanocrystals have a size distribution of about 20–30 nm.

After our structural analysis of the  $\text{Cs}_3\text{LuCl}_6$  metal halide,  $\text{Ce}^{3+}$ ,  $\text{Tb}^{3+}$ , and  $\text{Eu}^{3+}$  elements, which were widely researched as activators in phosphors,<sup>75</sup> as well as the  $\text{Sb}^{3+}$  element, which is actively studied in the lead-free perovskite research,<sup>76</sup> were used as activators to investigate  $\text{Cs}_3\text{LuCl}_6$ 's optical properties. XRD analysis was performed after each 5% doping of  $\text{Sb}^{3+}$ ,  $\text{Ce}^{3+}$ ,  $\text{Eu}^{3+}$ , and  $\text{Tb}^{3+}$  activators to determine whether the material retained the host structure of  $\text{Cs}_3\text{LuCl}_6$ . As shown in Figure 4f, the crystal structure of the host is maintained when the  $\text{Sb}^{3+}$ ,  $\text{Ce}^{3+}$ ,  $\text{Eu}^{3+}$ , and  $\text{Tb}^{3+}$  activators are doped. Subsequently, the optical properties of each doped activator were investigated. The steady-state photoluminescence (PL) and photoluminescence excitation (PLE) spectra are shown in Figure 4g.  $\text{Sb}^{3+}$ -doped  $\text{Cs}_3\text{LuCl}_6$  was measured upon 320 nm excitation and by monitoring the 520 nm broad emission.

Ce<sup>3+</sup>-doped Cs<sub>3</sub>LuCl<sub>6</sub> was measured upon 340 nm excitation and by monitoring the 380 nm broad emission. Eu<sup>3+</sup>-doped Cs<sub>3</sub>LuCl<sub>6</sub> was measured upon 290 nm excitation and by monitoring the 615 nm narrow emission. Finally, Tb<sup>3+</sup>-doped Cs<sub>3</sub>LuCl<sub>6</sub> was measured upon 280 nm excitation and by monitoring the 547 nm emission. This analysis supports the conclusion that Cs<sub>3</sub>LuCl<sub>6</sub> can be successfully functionalized through doping, thereby enabling its application for optoelectronic devices.

We also examined whether the Cs<sub>3</sub>LuCl<sub>6</sub> metal halide is thermally stable, as shown in our computation results. To confirm the crystalline phase was maintained under increasing heat, we conducted an *in situ* XRD measurement while varying the temperature conditions. When the temperature was raised to 250 °C, there was no significant change in the crystal structure except for the peak shift due to thermal expansion, and the main peaks of *in situ* XRD patterns are shown in Figure 4h. Subsequently, we conducted temperature-dependent PL measurements to assess the impact of thermal degradation on performance deterioration. For the purpose of comparison, these measurements additionally involved well-known 3D CsPbCl<sub>3</sub>, Cs<sub>3</sub>BiCl<sub>6</sub> with a lower Debye temperature (127 K), and 0D Cs<sub>3</sub>Bi<sub>2</sub>Cl<sub>9</sub> with an indirect band gap (Figure S11). Figure 4i shows the changes in PL intensity with increasing temperature. When doped with an activator of Ce<sup>3+</sup>, Cs<sub>3</sub>LuCl<sub>6</sub> exhibited the most stable PL, even at 150 °C. At 150 °C, Sb<sup>3+</sup>-, Ce<sup>3+</sup>-, Eu<sup>3+</sup>-, and Tb<sup>3+</sup>-doped Cs<sub>3</sub>LuCl<sub>6</sub> also showed thermally stable PL properties at 85%, 87%, 81%, and 92% of the PL intensity, respectively (Figure S12). These values exhibited a significant performance superiority over those of Sb<sup>3+</sup>-, Ce<sup>3+</sup>-, Eu<sup>3+</sup>-, and Tb<sup>3+</sup>-doped Cs<sub>3</sub>Bi<sub>2</sub>Cl<sub>9</sub> (Figure S13). This result indicates that the energy transfer to the luminescent center is stable at high temperatures, based on the stable 0D crystal structure of Cs<sub>3</sub>LuCl<sub>6</sub>, moderate Debye temperature of 149 K, and direct band gap type.

Later, we constructed a prototype white-light-emitting diode (WLED) to utilize a Cs<sub>3</sub>LuCl<sub>6</sub> material. This prototype WLED covered the entire visible spectrum and was created by mixing Cs<sub>3</sub>LuCl<sub>6</sub>:0.05 Sb<sup>3+</sup> with a wide green emission spectrum, Sr<sub>2</sub>MgSi<sub>2</sub>O<sub>7</sub>:Eu<sup>2+</sup> (SMS:Eu<sup>2+</sup>) for commercial blue phosphor, and K<sub>2</sub>SiF<sub>6</sub>:Mn<sup>4+</sup> (KSF:Mn<sup>4+</sup>) for commercial red phosphor. The mixture was then applied to a 365 nm UV LED chip as a color conversion layer. The spectrum in Figure 4j shows that an efficient color transformation occurred at wavelengths above 365 nm, covering all spectra between 400 and 700 nm. Additionally, the prototype operated successfully at flux currents ranging from 40 to 240 mA, with stable white light emission confirmed at a high emission rate of 28 lm W<sup>-1</sup> at 40 mA. The corresponding WLED produced white light with a color temperature of approximately 6000 K, as shown in Figure 4k.

In summary, the combination of high-throughput DFT calculations and machine learning allowed a rapid investigation of inorganic metal halides, with a particular focus on halide perovskites and their derivatives. This exploration presents a vast amount of information to guide experiments in material design as well as a comprehensive understanding of the properties of these materials. The successful validation of the new Cs<sub>3</sub>LuCl<sub>6</sub> discovered through our computation exploration suggests that our informatics can inspire experimental synthesis and demonstrate its potential to contribute to the development of new materials for optoelectronic and other practical applications. This study has expanded material

exploration beyond the existing perovskite structures, resulting in the implementation of a new inorganic metal halide and laying the groundwork for future advancement in materials with any complexity of structure and composition.

## ■ ASSOCIATED CONTENT

### SI Supporting Information

The Supporting Information is available free of charge at <https://pubs.acs.org/doi/10.1021/acsenergylett.3c01207>.

Materials, experimental and computational methodologies, additional theoretical analysis, and structural properties of Cs<sub>3</sub>LuCl<sub>6</sub> ([PDF](#))

Data set for training ML models ([ZIP](#))

Structure files of stable 255 metal halides ([ZIP](#))

## ■ AUTHOR INFORMATION

### Corresponding Authors

Won Bin Im – Division of Materials Science and Engineering, Hanyang University, Seoul 04763, Republic of Korea; [orcid.org/0000-0003-2473-4714](https://orcid.org/0000-0003-2473-4714); Email: [imwonbin@hanyang.ac.kr](mailto:imwonbin@hanyang.ac.kr)

Sung Beom Cho – Department of Materials Science and Engineering and Department of Energy Systems Research, Ajou University, Suwon 16499, Republic of Korea; [orcid.org/0000-0002-3151-0113](https://orcid.org/0000-0002-3151-0113); Email: [csb@ajou.ac.kr](mailto:csb@ajou.ac.kr)

### Authors

Hyeon Woo Kim – Division of Materials Science and Engineering, Hanyang University, Seoul 04763, Republic of Korea; Center of Materials Digitalization, Korea Institute of Ceramic Engineering and Technology (KICET), Jinju 52851, Republic of Korea

Joo Hyeong Han – Division of Materials Science and Engineering, Hanyang University, Seoul 04763, Republic of Korea

Hyunseok Ko – Center of Materials Digitalization, Korea Institute of Ceramic Engineering and Technology (KICET), Jinju 52851, Republic of Korea; [orcid.org/0000-0002-1891-6194](https://orcid.org/0000-0002-1891-6194)

Tuhin Samanta – Center of Materials Digitalization, Korea Institute of Ceramic Engineering and Technology (KICET), Jinju 52851, Republic of Korea

Dong Geon Lee – Division of Materials Science and Engineering, Hanyang University, Seoul 04763, Republic of Korea; Center of Materials Digitalization, Korea Institute of Ceramic Engineering and Technology (KICET), Jinju 52851, Republic of Korea

Dong Won Jeon – Department of Materials Science and Engineering and Department of Energy Systems Research, Ajou University, Suwon 16499, Republic of Korea

Woongchan Kim – Department of Materials Science and Engineering and Department of Energy Systems Research, Ajou University, Suwon 16499, Republic of Korea

Yong-Chae Chung – Division of Materials Science and Engineering, Hanyang University, Seoul 04763, Republic of Korea; [orcid.org/0000-0002-7545-4934](https://orcid.org/0000-0002-7545-4934)

Complete contact information is available at:

<https://pubs.acs.org/10.1021/acsenergylett.3c01207>

### Author Contributions

<sup>†</sup>H.W.K., J.H.H., and H.K. contributed equally to this work.

**Notes**

The authors declare no competing financial interest.

**ACKNOWLEDGMENTS**

This research was supported by National Research Foundation of Korea (RS-2023-00209910). We gratefully acknowledge support from the Ministry of Science and ICT (NRF-2020M3H4A3081867) and from the Samsung Research Funding & Incubation Center of Samsung Electronics under Project Number SRFC-TC2103-04.

**REFERENCES**

- (1) Jena, A. K.; Kulkarni, A.; Miyasaka, T. Halide Perovskite Photovoltaics: Background, Status, and Future Prospects. *Chem. Rev.* **2019**, *119* (5), 3036–3103.
- (2) Xiang, W.; Tress, W. Review on Recent Progress of All-Inorganic Metal Halide Perovskites and Solar Cells. *Adv. Mater.* **2019**, *31* (44), No. 1902851.
- (3) Ramasamy, P.; Lim, D.-H.; Kim, B.; Lee, S.-H.; Lee, M.-S.; Lee, J.-S. All-inorganic cesium lead halide perovskite nanocrystals for photodetector applications. *Chem. Commun.* **2016**, *52* (10), 2067–2070.
- (4) Wang, H.-P.; Li, S.; Liu, X.; Shi, Z.; Fang, X.; He, J.-H. Low-Dimensional Metal Halide Perovskite Photodetectors. *Adv. Mater.* **2021**, *33* (7), No. 2003309.
- (5) Liu, X.-K.; Xu, W.; Bai, S.; Jin, Y.; Wang, J.; Friend, R. H.; Gao, F. Metal halide perovskites for light-emitting diodes. *Nat. Mater.* **2021**, *20* (1), 10–21.
- (6) Lu, M.; Zhang, Y.; Wang, S.; Guo, J.; Yu, W. W.; Rogach, A. L. Metal Halide Perovskite Light-Emitting Devices: Promising Technology for Next-Generation Displays. *Adv. Funct. Mater.* **2019**, *29* (30), No. 1902008.
- (7) Dong, H.; Zhang, C.; Liu, X.; Yao, J.; Zhao, Y. S. Materials chemistry and engineering in metal halide perovskite lasers. *Chem. Soc. Rev.* **2020**, *49* (3), 951–982.
- (8) Liu, A.; Zhu, H.; Bai, S.; Reo, Y.; Zou, T.; Kim, M.-G.; Noh, Y.-Y. High-performance inorganic metal halide perovskite transistors. *Nat. Electron.* **2022**, *5* (2), 78–83.
- (9) Quan, L. N.; Rand, B. P.; Friend, R. H.; Mhaisalkar, S. G.; Lee, T.-W.; Sargent, E. H. Perovskites for Next-Generation Optical Sources. *Chem. Rev.* **2019**, *119* (12), 7444–7477.
- (10) Li, M.; Xia, Z. Recent progress of zero-dimensional luminescent metal halides. *Chem. Soc. Rev.* **2021**, *50* (4), 2626–2662.
- (11) Jodłowski, A.; Rodríguez-Padrón, D.; Luque, R.; de Miguel, G. Alternative Perovskites for Photovoltaics. *Adv. Energy Mater.* **2018**, *8* (21), No. 1703120.
- (12) Hou, J.; Wu, J.; Qin, Z.; Fang, Y.; Shen, L.; Qiao, X.; Dong, L.; Zhang, G.; Liu, Y.; Zhao, G.; et al. Lead-free halide  $\text{Cs}_2\text{MnCl}_4\text{:Cu}^+$  as a new phosphor for efficient green light emission. *J. Mater. Chem. C* **2023**, *11* (6), 2137–2143.
- (13) Han, J. H.; Samanta, T.; Park, Y. M.; Kim, H. J.; Manikanta Viswanath, N. S.; Kim, H. W.; Cha, B. K.; Cho, S. B.; Im, W. B. Highly Stable Zero-Dimensional Lead-Free Metal Halides for X-ray Imaging. *ACS Energy Lett.* **2023**, *8* (1), 545–552.
- (14) Samanta, T.; Viswanath, N. S. M.; Jang, S. W.; Min, J. W.; Cho, H. B.; Han, J. H.; Im, W. B. Thermally Stable Self-Trapped Assisted Single-Component White Light from Lead-Free Zero-Dimensional Metal Halide Nanocrystals. *Adv. Opt. Mater.* **2023**, *11*, No. 2202744.
- (15) Akkerman, Q. A.; Manna, L. What Defines a Halide Perovskite? *ACS Energy Lett.* **2020**, *5* (2), 604–610.
- (16) Creutz, S. E.; Liu, H.; Kaiser, M. E.; Li, X.; Gamelin, D. R. Structural Diversity in Cesium Bismuth Halide Nanocrystals. *Chem. Mater.* **2019**, *31* (13), 4685–4697.
- (17) Li, Y.; Yang, K. High-throughput computational design of halide perovskites and beyond for optoelectronics. *WIREs Comput. Mol. Sci.* **2021**, *11* (3), No. e1500.
- (18) Li, X.; Gao, X.; Zhang, X.; Shen, X.; Lu, M.; Wu, J.; Shi, Z.; Colvin, V. L.; Hu, J.; Bai, X.; et al. Lead-Free Halide Perovskites for Light Emission: Recent Advances and Perspectives. *Adv. Sci.* **2021**, *8* (4), No. 2003334.
- (19) Wei, Y.; Wang, W.; Wang, Z.; Yang, H.; You, X.; Zhao, Y.; Dang, P.; Lian, H.; Hao, J.; Li, G.; et al. Recent Progress of Bismuth Effect on All-Inorganic Lead-Free Metal Halide Derivatives: Crystals Structure, Luminescence Properties, and Applications. *Adv. Funct. Mater.* **2023**, *33* (2), No. 2205829.
- (20) Tao, Q.; Xu, P.; Li, M.; Lu, W. Machine learning for perovskite materials design and discovery. *npj Comput. Mater.* **2021**, *7* (1), 23.
- (21) Zhang, L.; He, M.; Shao, S. Machine learning for halide perovskite materials. *Nano Energy* **2020**, *78*, No. 105380.
- (22) Myung, C. W.; Hajibabaei, A.; Cha, J.-H.; Ha, M.; Kim, J.; Kim, K. S. Challenges, Opportunities, and Prospects in Metal Halide Perovskites from Theoretical and Machine Learning Perspectives. *Adv. Energy Mater.* **2022**, *12* (45), No. 2202279.
- (23) Jang, C.; Kim, K.; Nho, H.-W.; Lee, S. M.; Mubarok, H.; Han, J. H.; Kim, H.; Lee, D.; Jang, Y.; Lee, M. H.; et al. Synthesis of Thermally Stable and Highly Luminescent  $\text{Cs}_5\text{Cu}_3\text{Cl}_6\text{I}_2$  Nanocrystals with Nonlinear Optical Response. *Small* **2023**, *19*, No. 2206668.
- (24) Jun, T.; Sim, K.; Iimura, S.; Sasase, M.; Kamioka, H.; Kim, J.; Hosono, H. Lead-Free Highly Efficient Blue-Emitting  $\text{Cs}_3\text{Cu}_2\text{I}_5$  with 0D Electronic Structure. *Adv. Mater.* **2018**, *30*, No. e1804547.
- (25) Su, B.; Li, M.; Song, E.; Xia, Z. Sb<sup>3+</sup>-Doping in Cesium Zinc Halides Single Crystals Enabling High-Efficiency Near-Infrared Emission. *Adv. Funct. Mater.* **2021**, *31* (40), No. 2105316.
- (26) Kong, Q.; Yang, B.; Chen, J.; Zhang, R.; Liu, S.; Zheng, D.; Zhang, H.; Liu, Q.; Wang, Y.; Han, K. Phase Engineering of Cesium Manganese Bromides Nanocrystals with Color-Tunable Emission. *Angew. Chem., Int. Ed.* **2021**, *60* (36), 19653–19659.
- (27) Zhang, Y.; Liu, Y.; Xu, Z.; Ye, H.; Yang, Z.; You, J.; Liu, M.; He, Y.; Kanatzidis, M. G.; Liu, S. Nucleation-controlled growth of superior lead-free perovskite  $\text{Cs}_3\text{Bi}_2\text{I}_9$  single-crystals for high-performance X-ray detection. *Nat. Commun.* **2020**, *11* (1), 2304.
- (28) Noculak, A.; Morad, V.; McCall, K. M.; Yakunin, S.; Shynkarenko, Y.; Wörle, M.; Kovalenko, M. V. Bright Blue and Green Luminescence of Sb(III) in Double Perovskite  $\text{Cs}_2\text{MnInCl}_6$  ( $M = \text{Na}, \text{K}$ ) Matrices. *Chem. Mater.* **2020**, *32* (12), 5118–5124.
- (29) Chiara, R.; Ciftci, Y. O.; Queloz, V. I. E.; Nazeeruddin, M. K.; Grancini, G.; Malavasi, L. Green-Emitting Lead-Free  $\text{Cs}_4\text{SnBr}_6$  Zero-Dimensional Perovskite Nanocrystals with Improved Air Stability. *J. Phys. Chem. Lett.* **2020**, *11* (3), 618–623.
- (30) Lee, B.; Stoumpos, C. C.; Zhou, N.; Hao, F.; Malliakas, C.; Yeh, C.-Y.; Marks, T. J.; Kanatzidis, M. G.; Chang, R. P. H. Air-Stable Molecular Semiconducting Iodosalts for Solar Cell Applications:  $\text{Cs}_2\text{SnI}_6$  as a Hole Conductor. *J. Am. Chem. Soc.* **2014**, *136* (43), 15379–15385.
- (31) Fujimoto, Y.; Nakauchi, D.; Yanagida, T.; Koshimizu, M.; Asai, K. New Intrinsic Fast Scintillator: Cesium Praseodymium Chloride. *Sens. Mater.* **2022**, *34*, 629.
- (32) Liu, S.; Lyu, J.; Zhou, D.; Zhuang, X.; Shi, Z.; Sun, R.; Liu, L.; Wu, Y.; Liu, B.; Liu, D.; et al. Dual Modification Engineering via Lanthanide-Based Halide Quantum Dots and Black Phosphorus Enabled Efficient Perovskite Solar Cells with High Open-Voltage of 1.235 V. *Adv. Funct. Mater.* **2022**, *32* (19), No. 2112647.
- (33) Belsky, A.; Hellenbrandt, M.; Karen, V. L.; Luksch, P. New developments in the Inorganic Crystal Structure Database (ICSD): accessibility in support of materials research and design. *Acta Crystallogr. Sect. B* **2002**, *58*, 364–369.
- (34) Jain, A.; Ong, S. P.; Hautier, G.; Chen, W.; Richards, W. D.; Dacek, S.; Cholia, S.; Gunter, D.; Skinner, D.; Ceder, G.; et al. Commentary: The Materials Project: A materials genome approach to accelerating materials innovation. *APL Mater.* **2013**, *1* (1), No. 011002.
- (35) Hautier, G.; Fischer, C.; Ehrlacher, V.; Jain, A.; Ceder, G. Data Mined Ionic Substitutions for the Discovery of New Compounds. *Inorg. Chem.* **2011**, *50* (2), 656–663.
- (36) Wang, Z.; Ha, J.; Kim, Y. H.; Im, W. B.; McKittrick, J.; Ong, S. P. Mining Unexplored Chemistries for Phosphors for High-Color-Quality White-Light-Emitting Diodes. *Joule* **2018**, *2* (5), 914–926.

- (37) Sun, W.; Bartel, C. J.; Arca, E.; Bauers, S. R.; Matthews, B.; Orvánanos, B.; Chen, B.-R.; Toney, M. F.; Schelhas, L. T.; Tumas, W.; et al. A map of the inorganic ternary metal nitrides. *Nat. Mater.* **2019**, *18* (7), 732–739.
- (38) Wang, Y.; Richards, W. D.; Bo, S.-H.; Miara, L. J.; Ceder, G. Computational Prediction and Evaluation of Solid-State Sodium Superionic Conductors  $\text{Na}_x\text{P}_3\text{X}_{11}$  ( $X = \text{O}, \text{S}, \text{Se}$ ). *Chem. Mater.* **2017**, *29* (17), 7475–7482.
- (39) Zhu, H.; Hautier, G.; Aydemir, U.; Gibbs, Z. M.; Li, G.; Bajaj, S.; Pöhls, J.-H.; Broberg, D.; Chen, W.; Jain, A.; et al. Computational and experimental investigation of  $\text{TmAgTe}_2$  and  $\text{XYZ}_2$  compounds, a new group of thermoelectric materials identified by first-principles high-throughput screening. *J. Mater. Chem. C* **2015**, *3* (40), 10554–10565.
- (40) Ong, S. P.; Richards, W. D.; Jain, A.; Hautier, G.; Kocher, M.; Cholia, S.; Gunter, D.; Chevrier, V. L.; Persson, K. A.; Ceder, G. Python Materials Genomics ( pymatgen): A robust, open-source python library for materials analysis. *Comput. Mater. Sci.* **2013**, *68*, 314–319.
- (41) Ong, S. P.; Wang, L.; Kang, B.; Ceder, G. Li–Fe–P–O<sub>2</sub> Phase Diagram from First Principles Calculations. *Chem. Mater.* **2008**, *20* (5), 1798–1807.
- (42) Pal, J.; Bhunia, A.; Chakraborty, S.; Manna, S.; Das, S.; Dewan, A.; Datta, S.; Nag, A. Synthesis and Optical Properties of Colloidal  $\text{M}_3\text{Bi}_2\text{I}_9$  ( $\text{M} = \text{Cs}, \text{Rb}$ ) Perovskite Nanocrystals. *J. Phys. Chem. C* **2018**, *122* (19), 10643–10649.
- (43) Bass, K. K.; Estergreen, L.; Savory, C. N.; Buckeridge, J.; Scanlon, D. O.; Djurovich, P. I.; Bradforth, S. E.; Thompson, M. E.; Melot, B. C. Vibronic Structure in Room Temperature Photoluminescence of the Halide Perovskite  $\text{Cs}_3\text{Bi}_2\text{Br}_9$ . *Inorg. Chem.* **2017**, *56* (1), 42–45.
- (44) Tang, Y.; Liang, M.; Chang, B.; Sun, H.; Zheng, K.; Pullerits, T.; Chi, Q. Lead-free double halide perovskite  $\text{Cs}_3\text{BiBr}_6$  with well-defined crystal structure and high thermal stability for optoelectronics. *J. Mater. Chem. C* **2019**, *7* (11), 3369–3374.
- (45) Yang, H.; Cai, T.; Liu, E.; Hills-Kimball, K.; Gao, J.; Chen, O. Synthesis and transformation of zero-dimensional  $\text{Cs}_3\text{BiX}_6$  ( $X = \text{Cl}, \text{Br}$ ) perovskite-analogue nanocrystals. *Nano Res.* **2020**, *13* (1), 282–291.
- (46) Tailor, N. K.; Maity, P.; Saidaminov, M. I.; Pradhan, N.; Satapathi, S. Dark Self-Healing-Mediated Negative Photoconductivity of a Lead-Free  $\text{Cs}_3\text{Bi}_2\text{Cl}_9$  Perovskite Single Crystal. *J. Phys. Chem. Lett.* **2021**, *12* (9), 2286–2292.
- (47) Bianchini, M.; Wang, J.; Clément, R. J.; Ouyang, B.; Xiao, P.; Kitchaev, D.; Shi, T.; Zhang, Y.; Wang, Y.; Kim, H.; et al. The interplay between thermodynamics and kinetics in the solid-state synthesis of layered oxides. *Nat. Mater.* **2020**, *19* (10), 1088–1095.
- (48) Ali, M. S.; Das, S.; Abed, Y. F.; Basith, M. A. Lead-free  $\text{CsSnCl}_3$  perovskite nanocrystals: rapid synthesis, experimental characterization and DFT simulations. *Phys. Chem. Chem. Phys.* **2021**, *23* (38), 22184–22198.
- (49) Abrahams, I.; Demetriou, D. Z.; Kroemer, R. T.; Taylor, H.; Motevalli, M. Evidence for Cluster Orbital Formation in  $\text{CsSn}_2\text{X}_5$  Compounds ( $X = \text{Cl}, \text{Br}$ ). *J. Solid State Chem.* **2001**, *160* (2), 382–387.
- (50) Tan, Z.; Li, J.; Zhang, C.; Li, Z.; Hu, Q.; Xiao, Z.; Kamiya, T.; Hosono, H.; Niu, G.; Lifshitz, E.; et al. Highly Efficient Blue-Emitting Bi-Doped  $\text{Cs}_2\text{SnCl}_6$  Perovskite Variant: Photoluminescence Induced by Impurity Doping. *Adv. Funct. Mater.* **2018**, *28* (29), No. 1801131.
- (51) Andrews, R. H.; Clark, S. J.; Donaldson, J. D.; Dewan, J. C.; Silver, J. Solid-state properties of materials of the type  $\text{Cs}_4\text{MX}_6$  (where  $M = \text{Sn}$  or  $\text{Pb}$  and  $X = \text{Cl}$  or  $\text{Br}$ ). *J. Chem. Soc., Dalton Trans.* **1983**, No. 4, 767–770.
- (52) Gupta, S.; Bendikov, T.; Hodes, G.; Cahen, D.  $\text{CsSnBr}_3$ , A Lead-Free Halide Perovskite for Long-Term Solar Cell Application: Insights on  $\text{SnF}_2$  Addition. *ACS Energy Lett.* **2016**, *1* (5), 1028–1033.
- (53) Yuan, G.; Huang, S.; Niu, J.; Qin, S.; Wu, X.; Ding, H.; Lu, A. Compressibility of  $\text{Cs}_2\text{SnBr}_6$  by X-ray diffraction and Raman spectroscopy. *Solid State Commun.* **2018**, *275*, 68–72.
- (54) Marshall, K. P.; Walker, M.; Walton, R. I.; Hatton, R. A. Enhanced stability and efficiency in hole-transport-layer-free  $\text{CsSnI}_3$  perovskite photovoltaics. *Nat. Energy* **2016**, *1* (12), 16178.
- (55) Tan, L.; Wang, W.; Li, Q.; Luo, Z.; Zou, C.; Tang, M.; Zhang, L.; He, J.; Quan, Z. Colloidal syntheses of zero-dimensional  $\text{Cs}_4\text{SnX}_6$  ( $X = \text{Br}, \text{I}$ ) nanocrystals with high emission efficiencies. *Chem. Commun.* **2020**, *56* (3), 387–390.
- (56) Zhuo, Y.; Mansouri Tehrani, A.; Oliynyk, A. O.; Duke, A. C.; Brögch, J. Identifying an efficient, thermally robust inorganic phosphor host via machine learning. *Nat. Commun.* **2018**, *9* (1), 4377.
- (57) Xie, H.; Hao, S.; Bao, J.; Slade, T. J.; Snyder, G. J.; Wolverton, C.; Kanatzidis, M. G. All-Inorganic Halide Perovskites as Potential Thermoelectric Materials: Dynamic Cation off-Centering Induces Ultralow Thermal Conductivity. *J. Am. Chem. Soc.* **2020**, *142* (20), 9553–9563.
- (58) Zhihai, W.; Jiao, W.; Yanni, S.; Jun, W.; Yafei, H.; Pan, W.; Nengping, W.; Zhenfu, Z. Air-stable all-inorganic perovskite quantum dot inks for multicolor patterns and white LEDs. *J. Mater. Sci.* **2019**, *54* (9), 6917–6929.
- (59) Jin, J.; Peng, Y.; Xu, Y.; Han, K.; Zhang, A.; Yang, X.-B.; Xia, Z. Bright Green Emission from Self-Trapped Excitons Triggered by Sb<sup>3+</sup> Doping in  $\text{Rb}_4\text{CdCl}_6$ . *Chem. Mater.* **2022**, *34* (12), 5717–5725.
- (60) Xie, T.; Grossman, J. C. Crystal Graph Convolutional Neural Networks for an Accurate and Interpretable Prediction of Material Properties. *Phys. Rev. Lett.* **2018**, *120* (14), No. 145301.
- (61) De Angelis, F. The Impact of Machine Learning in Energy Materials Research: The Case of Halide Perovskites. *ACS Energy Lett.* **2023**, *8* (2), 1270–1272.
- (62) de Jong, M.; Chen, W.; Angsten, T.; Jain, A.; Notestine, R.; Gamst, A.; Sluiter, M.; Krishna Ande, C.; van der Zwaag, S.; Plata, J. J.; et al. Charting the complete elastic properties of inorganic crystalline compounds. *Sci. Data* **2015**, *2* (1), No. 150009.
- (63) Zhu, D.; Zaffalon, M. L.; Zito, J.; Cova, F.; Meinardi, F.; De Trizio, L.; Infante, I.; Brovelli, S.; Manna, L. Sb-Doped Metal Halide Nanocrystals: A 0D versus 3D Comparison. *ACS Energy Lett.* **2021**, *6* (6), 2283–2292.
- (64) Han, J. H.; Samanta, T.; Park, Y. M.; Cho, H. B.; Min, J. W.; Hwang, S. J.; Jang, S. W.; Im, W. B. Effect of self-trapped excitons in the optical properties of manganese-alloyed hexagonal-phased metal halide perovskite. *Chem. Eng. J.* **2022**, *450*, No. 138325.
- (65) Han, J. H.; Viswanath, N. S. M.; Park, Y. M.; Cho, H. B.; Jang, S. W.; Min, J. W.; Im, W. B. Zero-Thermal-Quenching Layered Metal Halide Perovskite. *Chem. Mater.* **2022**, *34* (12), 5690–5697.
- (66) Ilyas, B. M.; Elias, B. H. A theoretical study of perovskite  $\text{CsXCl}_3$  ( $X = \text{Pb}, \text{Cd}$ ) within first principles calculations. *Phys. B: Condensed Matter* **2017**, *510*, 60–73.
- (67) Evarestov, R. A.; Kotomin, E. A.; Senocrate, A.; Kremer, R. K.; Maier, J. First-principles comparative study of perfect and defective  $\text{CsPbX}_3$  ( $X = \text{Br}, \text{I}$ ) crystals. *Phys. Chem. Chem. Phys.* **2020**, *22* (7), 3914–3920.
- (68) Diroll, B. T.; Zhou, H.; Schaller, R. D. Low-Temperature Absorption, Photoluminescence, and Lifetime of  $\text{CsPbX}_3$  ( $X = \text{Cl}, \text{Br}, \text{I}$ ) Nanocrystals. *Adv. Funct. Mater.* **2018**, *28* (30), No. 1800945.
- (69) Liang, J.; Liu, J.; Jin, Z. All-Inorganic Halide Perovskites for Optoelectronics: Progress and Prospects. *Solar RRL* **2017**, *1* (10), No. 1700086.
- (70) Kim, H. W.; Ko, H.; Chung, Y.-C.; Cho, S. B. Heterostructural phase diagram of  $\text{Ga}_2\text{O}_3$ -based solid solution with  $\text{Al}_2\text{O}_3$ . *J. Eur. Ceram. Soc.* **2021**, *41* (1), 611–616.
- (71) Guo, Y.; Chen, B.; Ren, X.; Wang, F. Recent Advances in All-Inorganic Zero-Dimensional Metal Halides. *ChemPlusChem* **2021**, *86* (12), 1577–1585.
- (72) Jacobs, R.; Luo, G.; Morgan, D. Materials Discovery of Stable and Nontoxic Halide Perovskite Materials for High-Efficiency Solar Cells. *Adv. Funct. Mater.* **2019**, *29* (23), No. 1804354.
- (73) Sun, W.; Dacek, S. T.; Ong, S. P.; Hautier, G.; Jain, A.; Richards, W. D.; Gamst, A. C.; Persson, K. A.; Ceder, G. The thermodynamic scale of inorganic crystalline metastability. *Sci. Adv.* **2016**, *2* (11), No. e1600225.

(74) Samanta, T.; Mukurala, N.; Viswanath, N. S. M.; Han, J. H.; Cho, H. B.; Min, J. W.; Jung, S. W.; Park, Y.; Chung, W. J.; Im, W. B. Recent progress in lanthanide-based metal halide perovskites: Synthesis, properties, and applications. *Opt. Mater.: X* **2023**, *18*, No. 100238.

(75) Blasse, G.; Grabmaier, B. *Luminescent Materials*; Springer Science & Business Media, 2012.

(76) Saparov, B.; Hong, F.; Sun, J.-P.; Duan, H.-S.; Meng, W.; Cameron, S.; Hill, I. G.; Yan, Y.; Mitzi, D. B. Thin-film preparation and characterization of  $\text{Cs}_3\text{Sb}_2\text{I}_9$ : a lead-free layered perovskite semiconductor. *Chem. Mater.* **2015**, *27* (16), 5622–5632.